

Supporting Information

Electro-oxidation of Alcohols over Electrochemically Activated Nickel Alloys for Energy-saving Hydrogen Production

Ming Ni,^a Minyuan Tan,^b Kang Luo,^c Daochuan Jiang,^a Yupeng Yuan,^a Chuhong Zhu,^{a,*} Haiwei Du,^{a,*} and Hangjuan Ren^{d,*}

^a School of Materials Science and Engineering, Anhui University, Hefei 230601, China

^b National Synchrotron Radiation Laboratory, School of Nuclear Science and Technology, University of Science and Technology of China, Hefei 230029, China

^c Shanghai Leading Technology Co. Ltd, Shanghai 201807, China

^d School of Chemistry, Monash University, Clayton, Victoria 3800, Australia

Corresponding author email:

chzhu@ahu.edu.cn (C. Zhu)

haiwei.du@ahu.edu.cn (H. Du)

hangjuan.ren@monash.edu (H. Ren)



Figure S1 Photographs of the as-prepared Ni alloys before electrochemical activation, with a size of $1 \times 3 \text{ cm}^2$ and thickness of 0.2 mm.

Table S1 Nanoindentation data of the as-prepared Ni alloy.

Test point	Hardness (GPa)	Elastic modulus (GPa)
1	6.605	261.29
2	7.067	262.79
3	7.092	229.20

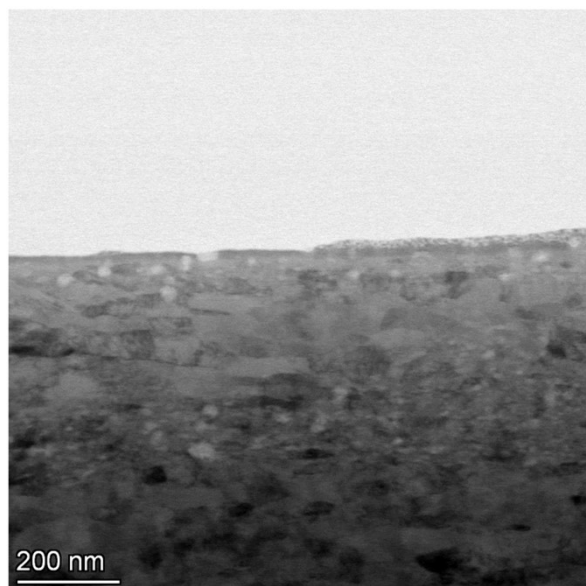


Figure S2 TEM image of the as-prepared Ni alloy before electrochemical activation.

Table S2 Elemental compositions of pristine and activated Ni alloys using ICP-OES.

	Elemental composition (wt%) ^a				
	Ni	Cr	Co	Mo	Fe
Pristine Ni alloys	62.11	20.23	12.19	7.49	0.68
Activated Ni alloy (after 200 CVs)	62.30	20.28	12.30	7.93	0.69

^a Average values obtained by two tests.

Table S3 Elemental compositions of the as-prepared Ni alloy using TEM EDX.

Elements	Atomic fraction (at%)	Mass fraction (wt%)
Ni	59.07	58.60
Cr	21.68	19.06
Co	12.66	12.61
Mo	5.19	8.42
Fe	1.39	1.32

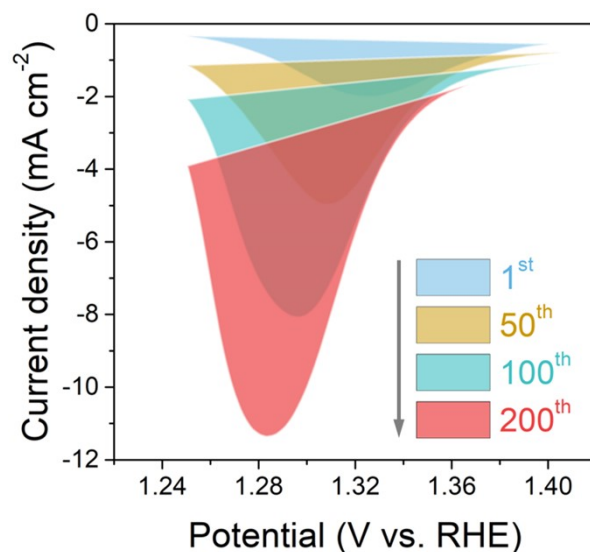


Figure S3 Backward CV curves of Ni alloy by different numbers of electrochemical activation cycles. The integrated area reflects the number of electrochemically active sites.

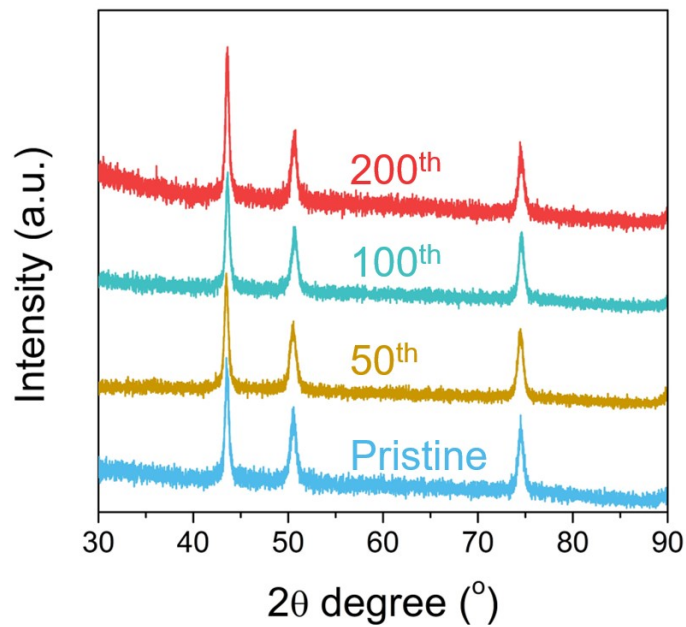


Figure S4 XRD patterns of Ni alloys before and after electrochemical activation through different CV cycles. No peak shift is observed after electrochemical activation.

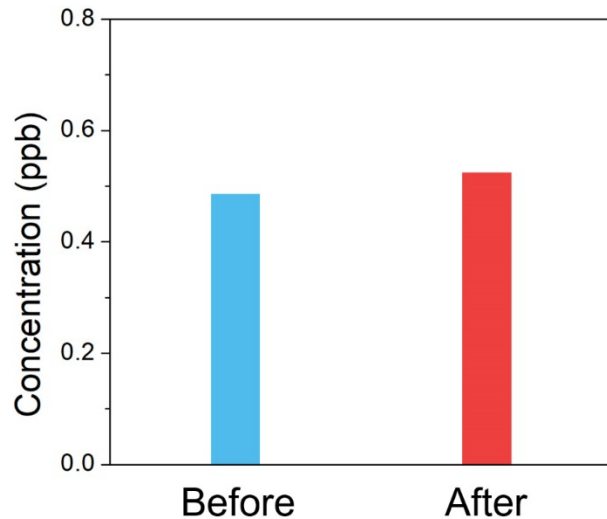


Figure S5 Concentration of metal elements in the solution before and after the total electrochemical activation.

Table S4 ICP-OES analysis of metal ion concentration in the solution before and after the electrochemical activation.

Metal elements	Concentration in the solution	Concentration in the solution
	before activation (ppb)	after activation (ppb)
Fe	0.437	0.4460
Co	0.009	0.0116
Ni	0.025	0.0430
Cr	0.009	0.0103
Mo	0.004	0.0137

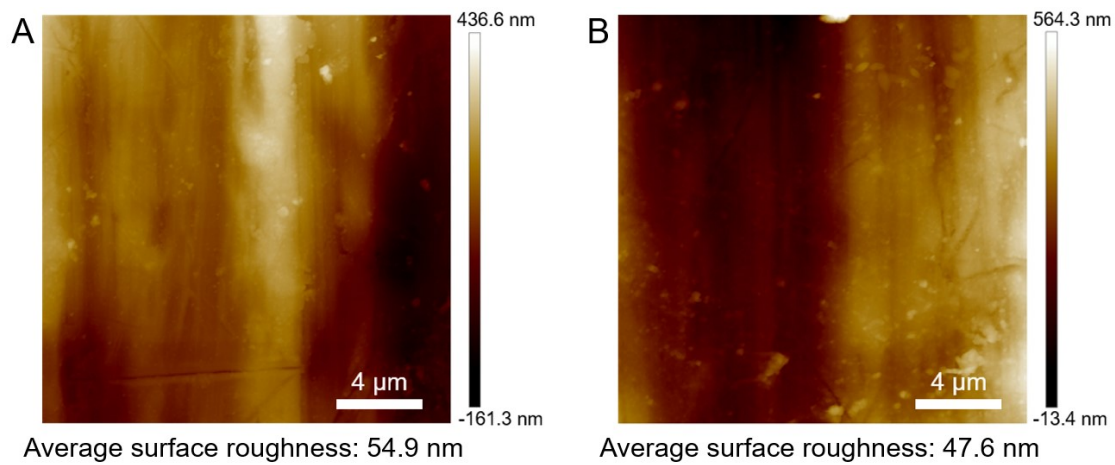


Figure S6 AFM images of the (a) pristine and (b) activated Ni alloys.

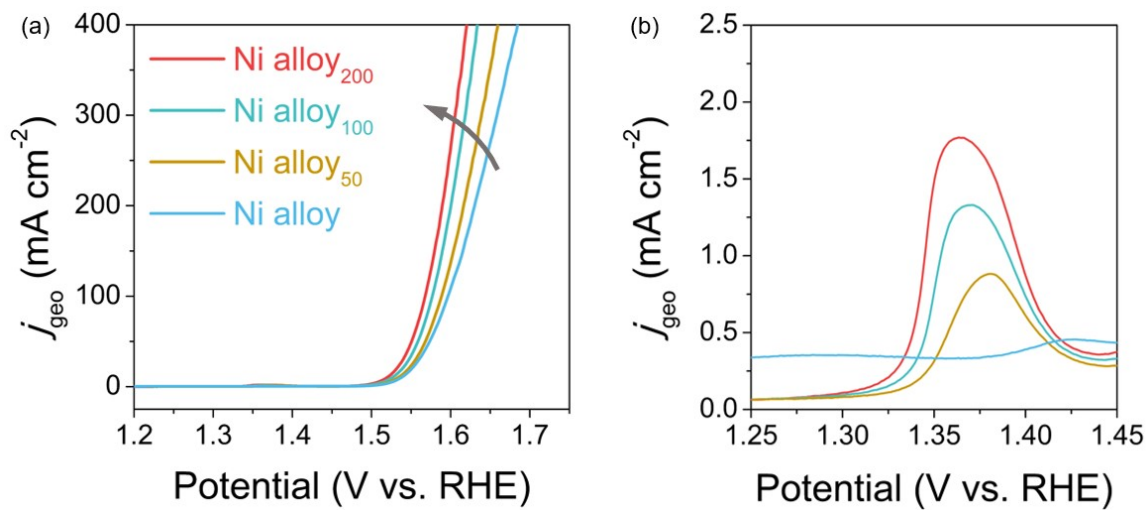


Figure S7 (a) LSV curves of the Ni alloy after different electrochemical activation cycles in 1 M KOH electrolyte at a scan rate of 5 mV s^{-1} . (b) The enlarge range between 1.25 ~ 1.45 V_{RHE}. The oxidation potential of $\text{Ni}^{2+}/\text{Ni}^{3+}$ negatively shifts with the increasing peak area, indicating the increased amount of Ni^{3+} (NiOOH).¹

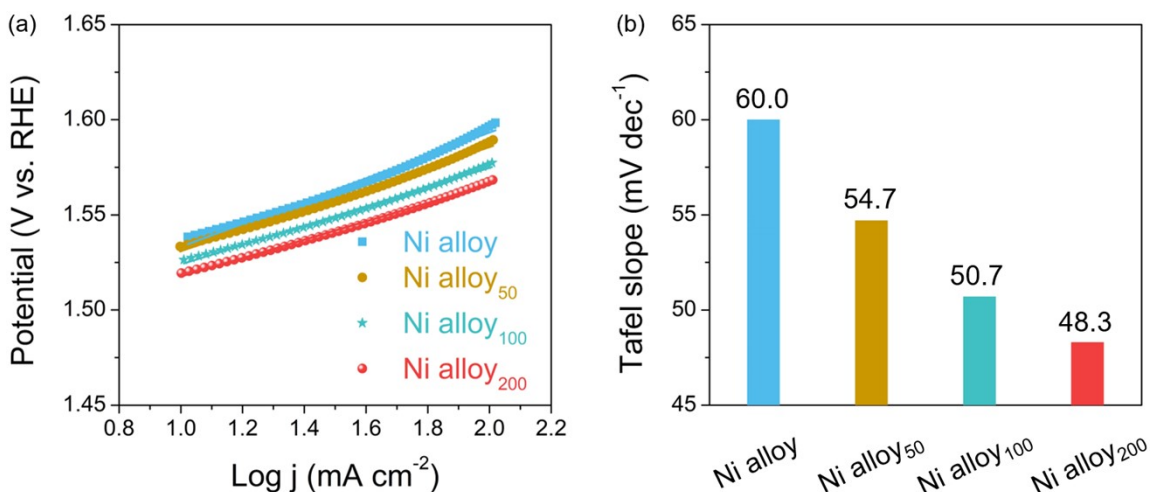


Figure S8 (a) Tafel plots and (b) comparison of Tafel slopes of Ni alloys before and after electrochemical activation.

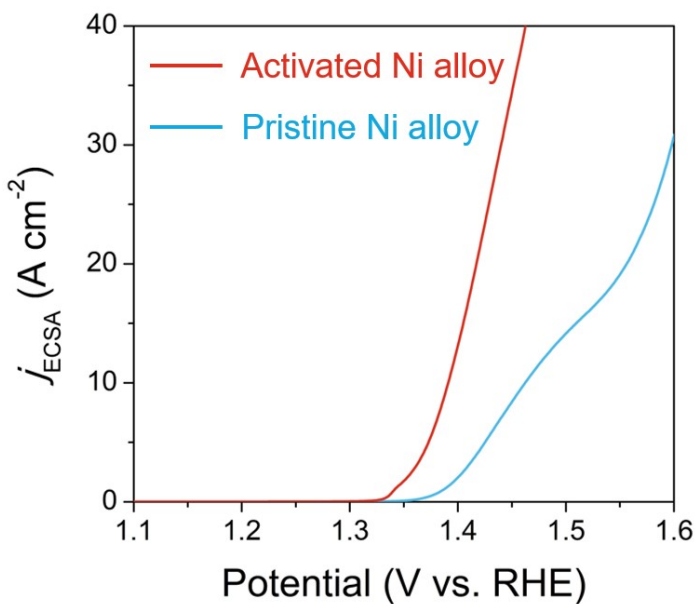


Figure S9 The ECSA normalized LSV curves of the pristine Ni alloy and the activated Ni alloy.

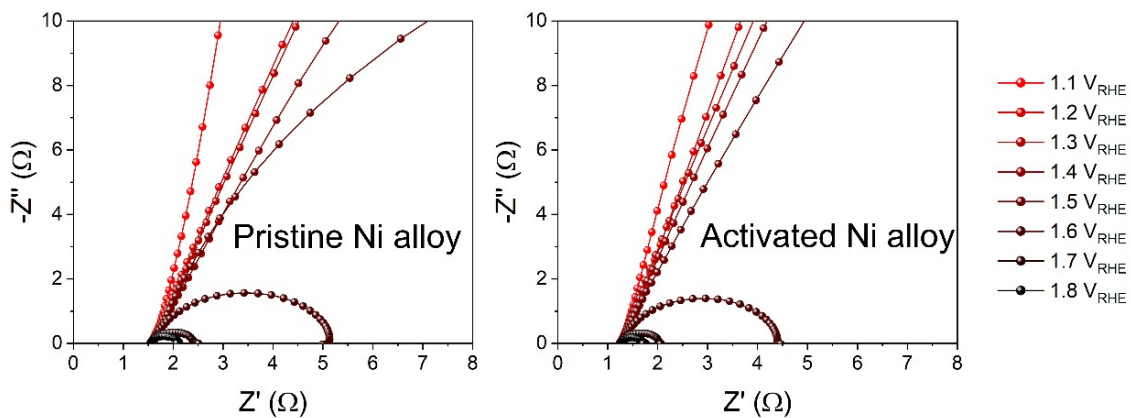


Figure S10 In-situ EIS spectra of the pristine Ni alloy and the activated Ni alloy.

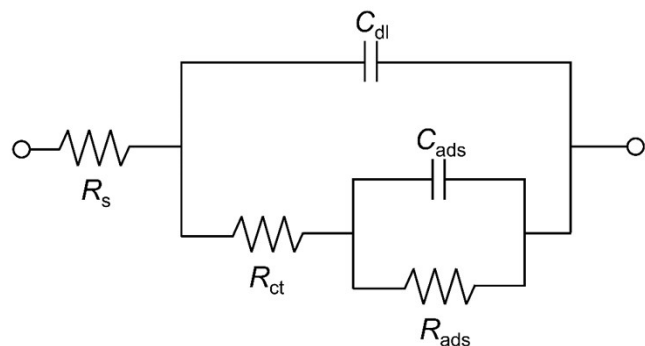


Figure S11 Equivalent circuit model used for EIS analyses. R_s : solution resistance, R_{ct} : charge transfer resistance, R_{ads} : resistance of interfacial adsorption, C_{dl} : double-layer capacitance, C_{ads} : capacitance of interfacial adsorption.²

Table S5 Resistance and capacitance obtained by analysing the *in-situ* EIS data of pristine Ni alloy and activated Ni alloy electrocatalyst (electrolyte: 1 M KOH).

	Potential (V _{RHE})	R_s (Ω)	R_{ct} (Ω)	C_{dl} (μF)	C_{ads} (μF)	R_{ads} (Ω)
Pristine Ni alloy	1.1	1.377	9967.4	0.059	0.079	9828
	1.2	1.363	4414	0.074	0.100	4307
	1.3	1.387	8399.05	0.088	0.137	8311
	1.4	1.403	6103.68	0.304	0.431	6039
	1.5	1.206	313.22	2.084	1.337	262.5
	1.6	1.138	2.491	1.419	4.380	0.927
	1.7	1.149	0.746	1.398	1.244	0.746
	1.8	1.14	0.298	1.324	9.402	0.043
Electrochemically activated Ni alloy	1.1	1.688	1007.2	0.068	0.122	818
	1.2	1.557	1011.6	0.085	0.184	826
	1.3	1.629	433.2	0.113	0.440	277
	1.4	1.405	93.78	6.202	6.595	27
	1.5	1.326	49.32	6.324	4.068	7.7
	1.6	1.274	3.117	3.878	5.150	1.902
	1.7	1.279	0.763	2.715	11.140	0.251
	1.8	1.286	0.451	2.749	835	0.043

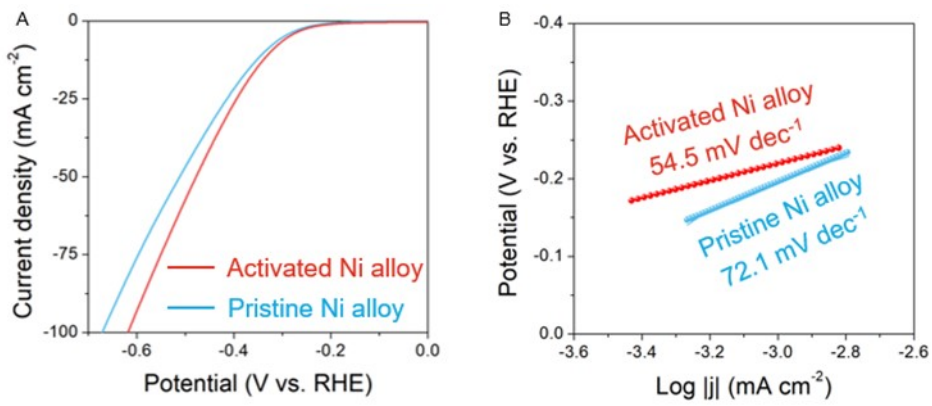


Figure S12 (a) HER LSV curves of pristine and electrochemically activated Ni alloys (electrolyte: 1 M KOH). (b) The corresponding Tafel plots.

Table S6 OER performance comparison between electrochemically activated Ni alloy and other transition metal based electrocatalysts in recently reported studies (electrolyte: 1 M KOH)

Electrocatalysts	Substrates	Overpotential @ 100 mA cm ⁻² (mV)	Tafel slope (mV dec ⁻¹)	Year	Ref.
Superwettable Ni ₃ S ₂ @Ni(II)	Nickel foam	~370	55	2023	[3]
a-Ni/CeO ₂ @NC	Carbon fiber paper	396	49	2023	[4]
Co-ZIF/CDs	Carbon cloth	401	147	2023	[5]
Co _{0.5} Fe _{0.5} LDH	Carbon cloth	~569	64.6	2023	[6]
CoO/CeO ₂	Nickel foam	~377	84	2023	[7]
NiFe/NiFeOOH with AMF	Glassy carbon electrode	~379	65.0	2023	[8]
Ru/Co ₃ O _{4-x}	Glassy carbon electrode	~442	86.9	2023	[9]
Ir@Zr-CoP	Carbon cloth	371	70.4	2023	[10]
H-ONSA	Nickel foam	~379	52.1	2023	[11]
Ru FeNi@NLC	Carbon paper	340	72	2023	[12]
FeCoCuMnRuB	Glassy carbon electrode	323	61	2024	[13]
HEP@SWCNTs	Glassy carbon electrode	~316	56	2024	[14]
Activated Ni alloy	Ni alloy	337	48.3	2024	This work

NC: nitrogen-doped carbon;

CDs: carbon dots;

LDH: layered double hydroxide;

AMF: alternating magnetic field;

ONSA: orthogonal nanosheets with single-crystalline arrays;

HEP: high-entropy metal phosphide;

SWCNTs: single-wall carbon nanotubes;

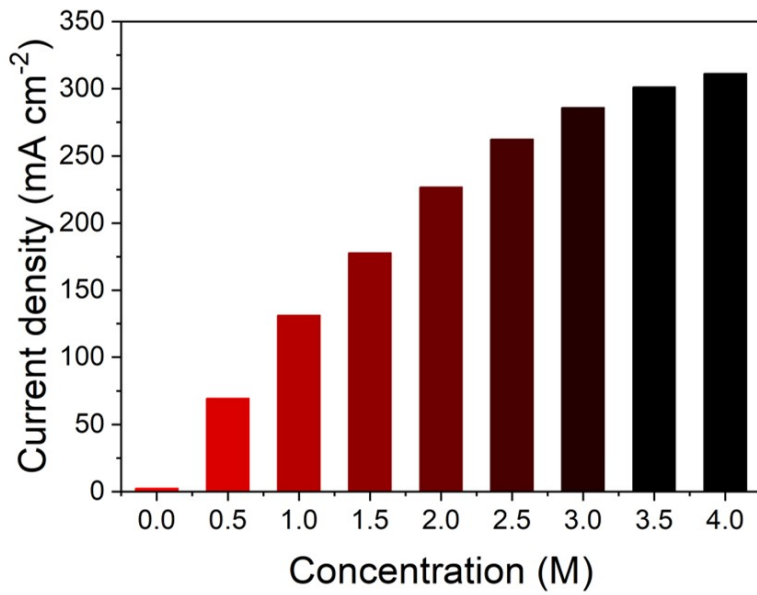


Figure S13 Current densities of the activated Ni alloy recorded at $1.5 \text{ V}_{\text{RHE}}$ when different concentrations of methanol are added.

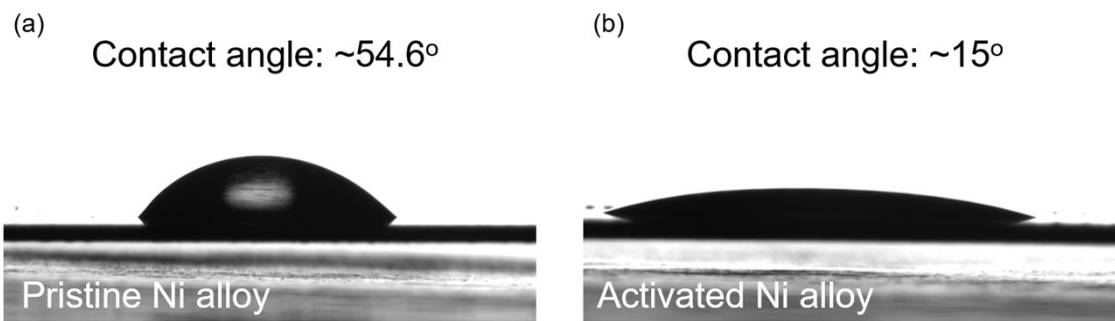


Figure S14 Contact angle measurement of (a) pristine and (b) activated Ni alloy. Solution: 1 M KOH + 2 M MeOH.

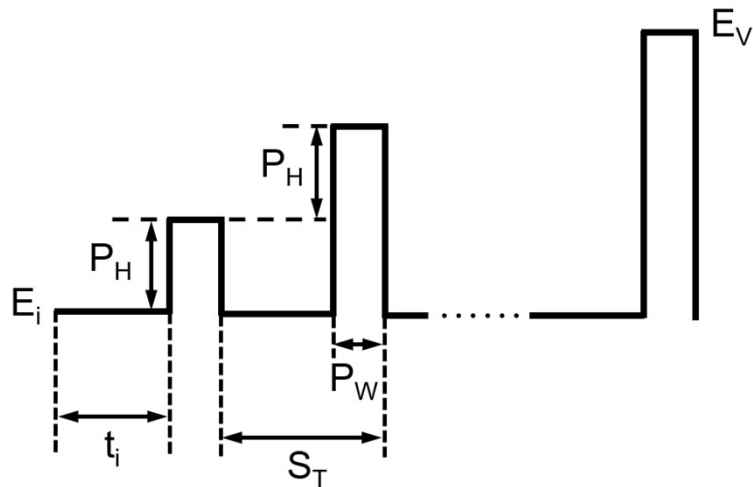


Figure S15 Experimental parameters of normal pulse voltammograms. E_i (initial potential) = 1.275 V_{RHE}; P_H (pulse height) = 0.1 mV; P_W (pulse width) = 10 ms; t_i (initial time) = 300 ms; S_T (step time) = 300 ms; E_V : final potential.

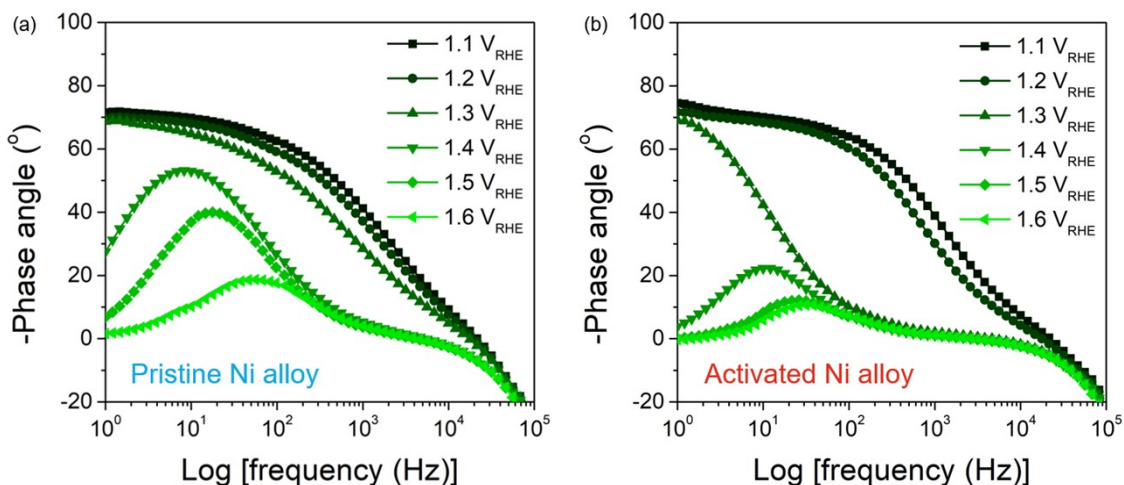


Figure S16 Phase angle variation recorded in 1 M KOH + 2 M MeOH at different potentials:
 (a) pristine and (b) activated Ni alloy.

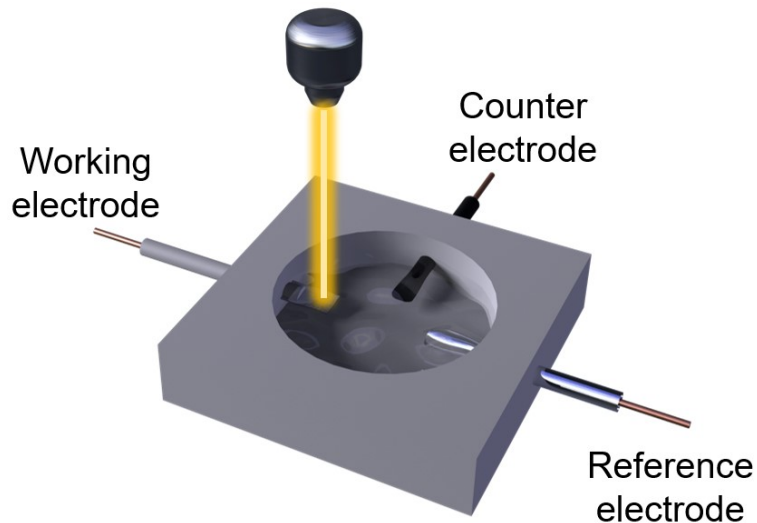


Figure S17 Schematic of setup of *in-situ* Raman test.

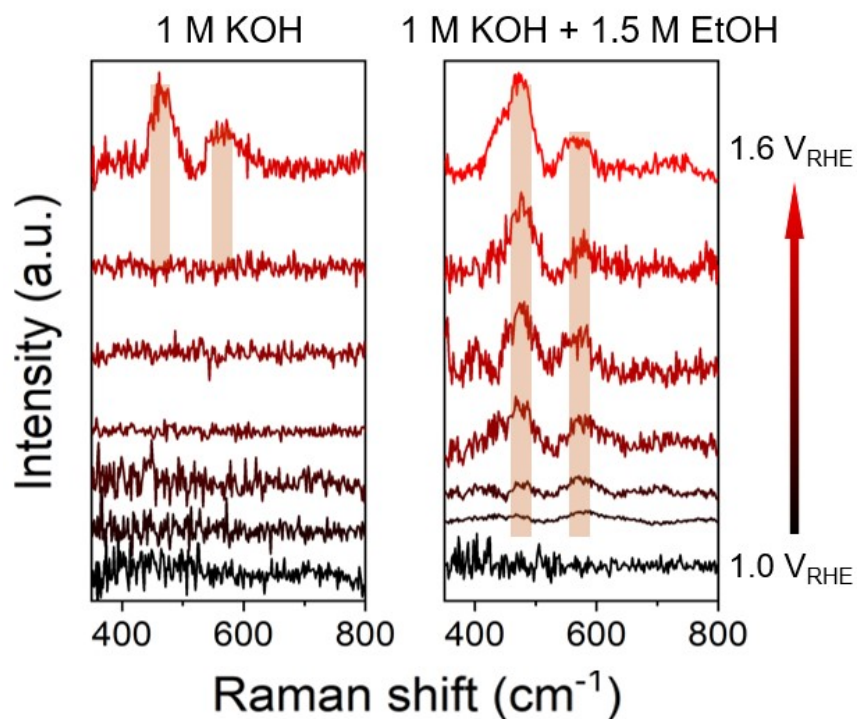


Figure S18 Raw data of *in-situ* Raman spectra of activated Ni alloys recorded in (a) 1 M KOH or (b) 1 M KOH + 1.5 M EtOH.

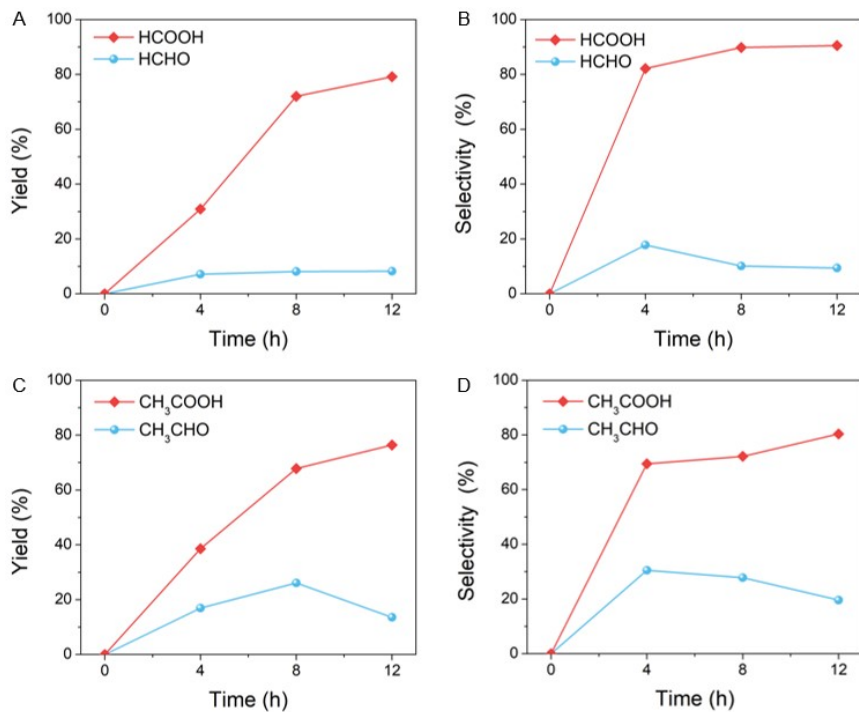


Figure S19 Yield and selectivity of the oxidation products from (a, b) methanol and (c, d) ethanol over the activated Ni alloy.

References

1. R. A. Márquez, K. Kawashima, Y. J. Son, R. Rose, L. A. Smith, N. Miller, O. A. Carrasco Jaim, H. Celio and C. B. Mullins, *ACS Appl. Mater. Interfaces*, 2022, **14**, 42153-42170.
2. F. Dionigi, Z. Zeng, I. Sinev, T. Merzdorf, S. Deshpande, M. B. Lopez, S. Kunze, I. Zegkinoglou, H. Sarodnik, D. Fan, A. Bergmann, J. Drnec, J. F. d. Araujo, M. Gliech, D. Teschner, J. Zhu, W.-X. Li, J. Greeley, B. R. Cuenya and P. Strasser, *Nat. Commun.*, 2020, **11**, 2522.
3. F. Zhang, R. Zhao, Y. Wang, L. Han, J. Gu, Z. Niu, Y. Yuan, N. Qu, J. Meng and D. Wang, *Chem. Eng. J.*, 2023, **452**, 139513.
4. Z. Pei, H. Zhang, Z.-P. Wu, X. F. Lu, D. Luan and X. W. Lou, *Sci. Adv.*, 2023, **9**, eadh1320.
5. Q. Hong, Y. Wang, R. Wang, Z. Chen, H. Yang, K. Yu, Y. Liu, H. Huang, Z. Kang and P. W. Menezes, *Small*, 2023, **19**, 2206723.
6. S. Shankar Naik, J. Theerthagiri, F. S. Nogueira, S. J. Lee, A. Min, G.-A. Kim, G. Maia, L. M. C. Pinto and M. Y. Choi, *ACS Catal.*, 2023, **13**, 1477-1491.
7. H. Liu, H. Duan, J. Yu, C. Qiu, R. Yu, J. Gao, S. Li, X. Du, Z. Si and S. Yang, *ACS Mater. Lett.*, 2022, **4**, 2572-2578.
8. D. Peng, C. Hu, X. Luo, J. Huang, Y. Ding, W. Zhou, H. Zhou, Y. Yang, T. Yu, W. Lei and C. Yuan, *Small*, 2023, **19**, 2205665.
9. C.-Z. Yuan, S. Wang, K. San Hui, K. Wang, J. Li, H. Gao, C. Zha, X. Zhang, D. A. Dinh, X.-L. Wu, Z. Tang, J. Wan, Z. Shao and K. N. Hui, *ACS Catal.*, 2023, **13**, 2462-2471.
10. Q. P. Ngo, T. T. Nguyen, Q. T. T. Le, J. H. Lee and N. H. Kim, *Adv. Energy Mater.*, 2023, **13**, 2301841.
11. Y. Zou, C. Liu, C. Zhang, L. Yuan, J. Li, T. Bao, G. Wei, J. Zou and C. Yu, *Nat. Commun.*, 2023, **14**, 5780.
12. X. Lin, J. Liu, X. Qiu, B. Liu, X. Wang, L. Chen and Y. Qin, *Angew. Chem. Int. Ed.*, 2023, **62**, e202306333.
13. L. Liu, T. Liu, C. Xu, W. Zhao, J. Fan, J. Liu, X. Ma and W. Fu, *Nano Lett.*, 2024, **24**, 2831-2838.
14. J. Du, S. Liu, Y. Liu, G. Wu, X. Liu, W. Zhang, Y. Zhang, X. Hong, Q. Li and L. Kang, *J. Am. Chem. Soc.*, 2024, **146**, 8464-8471.